

Three-dimensional position measurement of a levitated nanoparticle in a vacuum by a Dove prism

Yu Zheng (郑瑜)^{1,2} and Fangwen Sun (孙方稳)^{1,2,*}

¹CAS Key Laboratory of Quantum Information, University of Science and Technology of China, Hefei 230026, China

²CAS Center for Excellence in Quantum Information and Quantum Physics, University of Science and Technology of China, Hefei 230026, China

*Corresponding author: fwsun@ustc.edu.cn

Received December 24, 2018; accepted March 21, 2019; posted online June 4, 2019

Forward-scattering-light interferometry has become the most commonly used position detection scheme in optical levitation systems. Usually, three-set detectors are required to obtain the three-dimensional motion information. Here, we simplify the three-set detectors to one set by inserting a Dove prism. We investigate the role of a Dove prism in the position measurement process with an optical levitation system in vacuum. The relationship between the power spectral density and the rotation angle of a Dove prism is experimentally demonstrated and analyzed. This work shows that the Dove prism can greatly reduce the complexity of the experimental setup, which can be applied to compact optical levitation systems for studies in metrology, quantum physics, and biology.

OCIS codes: 090.1970, 140.7010.
doi: 10.3788/COL201917.060901.

Levitation systems in vacuum, especially optical levitation, have become one of the most popular optomechanical systems, due to low damping, isolation from the environment, and outstanding motion control ability^[1]. Many basic physical topics have been investigated in this system such as Brown motion on the nanoscale^[2], ultra-weak force detection^[3–5], mechanical cooling of nanoparticles^[6,7], and microscopic thermodynamics^[8,9]. The prospect of a mesoscopic quantum platform in levitation systems has also been shown^[10–14].

For all levitation experiments, it is fundamentally necessary to acquire the position of the levitated particle. In all the position detection schemes, forward-scattering-light interferometry combined with balanced photodetectors^[2,15] has become the most commonly used scheme due to its large bandwidth and high sensitivity.

In the forward-scattering-light interferometry scheme, position information is hidden in the interference pattern between the trapping laser and the scattering light from the trapped particles^[16–19]. Due to the asymmetry of the potential well^[20], the movement of the trapped particle can be separated into three independent components with their motion directions perpendicular to each other. For a Gaussian beam trapping laser, the directions of the three components are respectively parallel to the propagation direction of the beam (set as the Z axis), the polarization direction of the laser (set as the X axis), and a direction perpendicular to the plane of the other two directions (set as the Y axis). To extract all the 3D position information in X - Y - Z axes from the interference pattern^[6,7], first, a set of beam splitters is used to divide the forward-scattering light into 3 parts. Usually, a D-shaped mirror is applied to split one part of the light beams in two halves from the center along the X axis. A balanced photodetector

measures the light intensity of the two halves of the light beams separately and outputs the difference, which is proportional to the displacement distance from the equilibrium position in the Y direction. The method for measuring the movement along the X direction is similar, except that the beam is split along the Y axis. The intensity difference between the forward-scattering light and a reference beam sample from the trapping laser is proportional to the displacement distance along the Z axis, which can be recorded to present the movement along the Z direction.

Although the conventional forward-scattering-light interferometry scheme is sophisticated, there are still two improvements that can be done. First, it is unnecessary to set three balanced detectors if we do not need to record all the three-dimensional (3D) movements simultaneously. Second, due to the residual internal stress of the optical component, the polarization of the trapping laser may deviate from the original direction. It may make the direction of the independent-moving axis deviate and introduce a cross talk from other axis motion in the position signal. Eliminating the cross talk by adjusting the D-shaped mirror is very inconvenient due to difficulties in the re-adjustment of subsequent optical components that are used to couple the light into the photodiode. Here, instead of rotating the D-shaped mirror to adjust the split angle on the forward-scattering light, we can rotate the light beam by inserting a Dove prism into the light path between the optical trap and the D-shaped mirror.

As shown in Fig. 1(a), the Dove prism can flip the image that propagates along its longitudinal axis, and when the Dove prism is rotated by φ around its longitudinal axis, the flipped image will be rotated by 2φ in the same direction around the axis of the Dove prism^[21].

Assuming the rotation angle of the Dove prism is 0° when the two trapezoidal faces are perpendicular to the X axis, the outlet light pattern is just flipped vertically without rotation. It has been proved that the intensity difference between the left and right half is proportional to the displacement distance of the trapped particle from the equilibrium position in the X axis^[18]. We can get that

$$I_R - I_L = N_x x_0, \quad (1)$$

where x_0 is the displacement in the X axis, N_x is the conversion factor between the intensity and displacement, and I_R (I_L) is the intensity of the right (left) half of the forward-scattering-light beam. It means that

$$I_R = \int_0^{r_{\max}} \int_{-\frac{\pi}{2}}^{\frac{\pi}{2}} I(r, \theta, r_0, \theta_0) d\theta dr, \quad (2)$$

$$I_L = \int_0^{r_{\max}} \int_{\frac{\pi}{2}}^{\frac{3\pi}{2}} I(r, \theta, r_0, \theta_0) d\theta dr, \quad (3)$$

where $I(r, \theta, r_0, \theta_0)$ is the intensity distribution on the detection plane without a Dove prism. (r_0, θ_0) and (x_0, y_0) are the position coordinates of the trapped particle in the circular coordinate or the Cartesian coordinates on the X - Y plane. r_{\max} depends on the numerical aperture (NA) of the condenser and can be assumed to be infinity here.

If we rotate the Dove prism by $\pi/4$, the intensity distribution on the detection plane will be flipped and rotated by $\pi/2$ around the Z axis. The intensity of left and right half is

$$I'_R = \int_0^{r_{\max}} \int_{-\pi}^0 I(r, \theta, r_0, \theta_0) d\theta dr, \quad (4)$$

$$I'_L = \int_0^{r_{\max}} \int_0^\pi I(r, \theta, r_0, \theta_0) d\theta dr. \quad (5)$$

It means that the laser intensity on the right photodiode is from the bottom half of the forward-scattering-light beam, and the intensity on the left is from the top half. So, we can get that

$$I'_R - I'_L = I_{\text{down}} - I_{\text{up}} = -N_y y_0, \quad (6)$$

where y_0 is the displacement in the Y axis, N_y is the conversion factor between the intensity and the displacement, and I_{down} (I_{up}) is the intensity of the lower (upper) half of the forward-scattering-light beam. Therefore, from Eqs. (1) and (6), we can measure the displacement in the X and Y axis on the same balanced photodetector by rotating the Dove prism.

Since the movements along the X and Y directions are independent, we can get the output of the balanced detector as

$$I_R^{\varphi_0} - I_L^{\varphi_0} = N_x x_0 \cos(2\varphi_0) - N_y y_0 \sin(2\varphi_0), \quad (7)$$

when the Dove prism is rotated by φ_0 .

In the experiment, as shown in Fig. 1(b), a 200 mW 1064 nm TEM00 Gaussian laser with polarization along the X axis is focused by an objective (NA = 0.9) in a vacuum chamber. Silicon nanospheres are dispersed in ethanol and sent to the trapping position by an ultrasonic nebulizer. The forward-scattering-light that is collected by an aspheric lens (NA = 0.546) passes through the Dove prism (Thorlabs PM992M-B) and is split by a D-shaped mirror in half from the center along the Y axis. A home-made balanced photodetector (3 MHz bandwidth, AC couple) measures the light intensity difference between the two halves. The signal voltage from the balanced photodetector is recorded by a 250 MS/s digitizer (Spectrum M4i.4421-x8) and processed with MATLAB.

To measure all 3D positions of the trapped nanosphere, we set the Dove prism with its trapezoidal face perpendicular to the X axis and fine rotate the prism until the cross talk from the Y axis motion is minimal according to the power spectral density (PSD). Here we mark the rotation angle of the prism as 0° . Now, the output signal voltage of balanced detector is proportional to the displacement from the equilibrium position on the X axis. Then the prism is rotated by 45° . The signal voltage will be proportional to the displacement on the Y axis. Last, we remove the D-shaped mirror to put all the forward-scattering light into one photodiode of the detector. In this case, the signal voltage is proportional to the displacement on the Z axis. The PSD of movement in the X - Y - Z axis in vacuum is shown in Fig. 2, which can be fitted with^[22]

$$S(\omega) = \frac{2k_B T}{M\Omega^2} \frac{\Omega^2 \Gamma_0}{(\Omega^2 - \omega^2)^2 + \omega^2 \Gamma_0^2}, \quad (8)$$

where Ω is the eigen angular frequency of the trapped nanosphere, Γ_0 is the damping rate, M is the mass of the nanosphere, T is the environment temperature, and k_B is the Boltzmann constant.

To get the conversion factor between the signal voltage and the actual displacement, we need to know the mass of the trapped particles. Here, we can obtain the damping rate by fitting the PSD and recording the damping rate at different air pressures, which can be fitted by^[23]

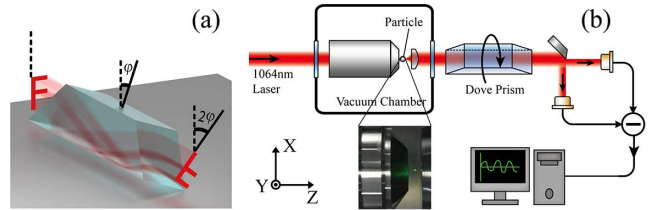


Fig. 1. Schematic of 3D position detection with a Dove prism. (a) Light propagating along the longitudinal axis is inverted by 180° and the angle of rotation of the image is twice that of the rotation angle of the prism. (b) Schematic of the experiment setup. The green spot in the inset is a trapped particle that is illuminated by another 532 nm laser.

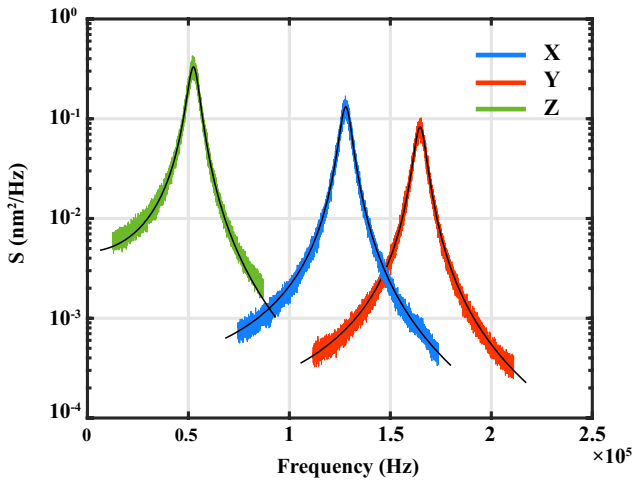


Fig. 2. PSD of the motion in the X - Y - Z axis. The resonance frequencies are $\Omega = 52.7$ kHz, 128.0 kHz, and 164.8 kHz, respectively. The black lines are fitting curves according to Eq. (8). The air pressure in the vacuum chamber is 8.1 mbar. The diameter of the trapped nanosphere is 154 ± 1 nm.

$$\Gamma_0 = \frac{6\pi\eta R}{M} \frac{0.619}{0.619 + Kn} (1 + c_K), \quad (9)$$

where R is the radius of the nanosphere, $c_K = 0.31Kn/(0.785 + 1.152Kn + Kn^2)$, η is the viscosity coefficient of air, and $Kn = \bar{l}/R$ is the Knudsen number. $\bar{l} = k_B T / (\sqrt{2}\pi d^2 p)$ is the mean free path of air molecules, where p is the air pressure and d is the mean diameter of the air molecules. As shown in Fig. 3, by setting the density of the particle to be 1900 kg/m^3 , we can get that the diameter of the trapped particle is 154 ± 1 nm. The mass is $(3.63 \pm 0.07) \times 10^{-18} \text{ kg}$.

In order to investigate the relationship between the measured signal and the rotation angle of the prism, we can make a Fourier transformation for Eq. (7) as

$$\mathcal{F}(I_0(t)) = N_x \cos(2\varphi_0) \mathcal{F}(x_0(t)) - N_y \sin(2\varphi_0) \mathcal{F}(y_0(t)), \quad (10)$$

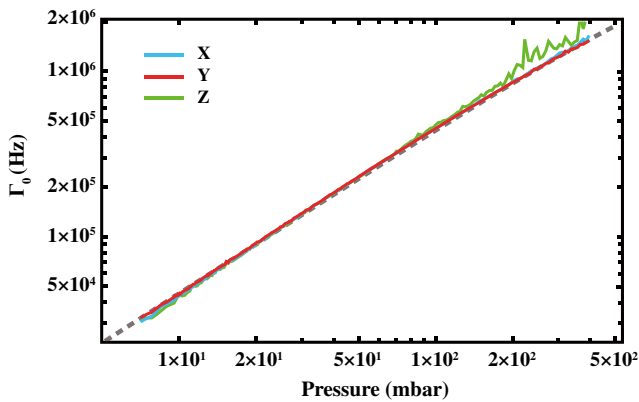


Fig. 3. Damping rate decreases with the air pressure. The dashed line is a fit according to Eq. (9).

where I_0 is the output of the balanced detector. The PSDs of the X and Y directional motions can be written as^[22]

$$S_x(\omega) = |\mathcal{F}(x_0(t))|^2 / T_{\text{rec}}, \quad (11)$$

$$S_y(\omega) = |\mathcal{F}(y_0(t))|^2 / T_{\text{rec}}, \quad (12)$$

where T_{rec} is the recording duration. So, the PSD of the recorded signal can be written as

$$\begin{aligned} S_I(\omega) &= |\mathcal{F}(I_0(t))|^2 / T_{\text{rec}} \\ &= \{N_x^2 \cos^2(2\varphi_0) |\mathcal{F}(x_0(t))|^2 \\ &\quad + N_y^2 \sin^2(2\varphi_0) |\mathcal{F}(y_0(t))|^2 \\ &\quad - N_x N_y \sin(2\varphi_0) \cos(2\varphi_0) [\overline{\mathcal{F}(x_0(t))} \mathcal{F}(y_0(t)) \\ &\quad + \mathcal{F}(x_0(t)) \overline{\mathcal{F}(y_0(t))}]\} / T_{\text{rec}}. \end{aligned} \quad (13)$$

Because the PSD output is an average of several samples to reduce random noise and the phase difference between X and Y directional motions is random, we can get

$$\langle \overline{\mathcal{F}(x_0(t))} \mathcal{F}(y_0(t)) + \mathcal{F}(x_0(t)) \overline{\mathcal{F}(y_0(t))} \rangle = 0. \quad (14)$$

Therefore, Eq. (13) can be simplified to

$$S_I(\omega) = N_x^2 A_x S_x(\omega) + N_y^2 A_y S_y(\omega), \quad (15)$$

where $A_x = \cos^2(2\varphi_0)$, and $A_y = \sin^2(2\varphi_0)$. It means that the PSD of the detected data after the Dove prism at angle φ_0 can be decomposed into an X part and a Y part, with scale factors $\cos^2(2\varphi_0)$ and $\sin^2(2\varphi_0)$, respectively.

We record the PSD of position signal at different angles of the Dove prism, as shown in Fig. 4. During the rotation of the Dove prism from the original angle, the peak of the X resonance frequency is decreasing and the peak of the Y

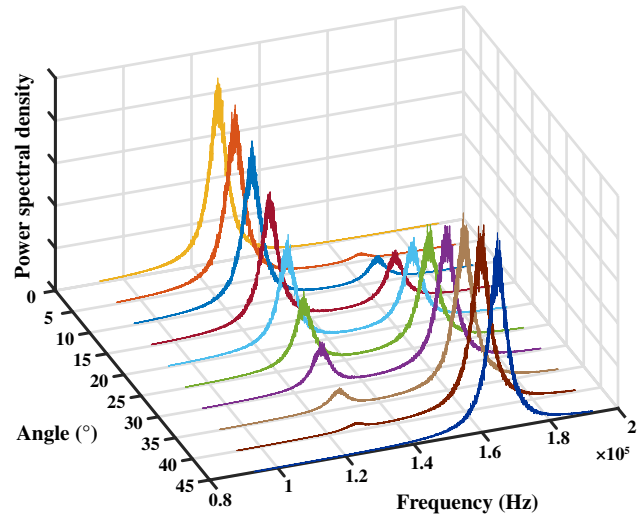


Fig. 4. PSD of the position signal at different rotation angles of the Dove prism.

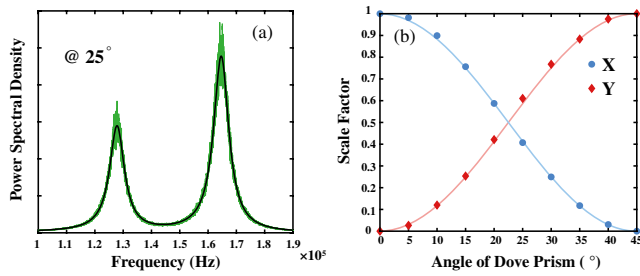


Fig. 5. Peak height of the X and Y frequency parts in the PSD according to the rotation angle of the Dove prism. (a) The PSD when the Dove prism rotation angle is 25° . The black line is the fitting curve according to Eq. (15). (b) The scale factors of the X and Y parts according to Eq. (15) vary with the rotation angle of the Dove prism. The blue and red lines demonstrate $\cos^2(2\varphi)$ and $\sin^2(2\varphi)$, respectively. φ is the rotation angle of the Dove prism.

resonance frequency is rising. When the rotation angle is 45° , the peak of the Y resonance frequency reaches a maximum and the peak of X resonance frequency is negligible. Figure 5(b) shows the normalized scale factors of the X part and the Y part in Eq. (15) changing with the rotation angle of the Dove prism.

In conclusion, we experimentally measured the position of the optical trapped particle in vacuum along X , Y and Z with one balanced detector by inserting a Dove prism and investigated the effect of the Dove prism on the position signal at different rotation angles. This experimental scheme can simplify the measurement system when it is not necessary to obtain the position information of different dimensions at the same time. This Dove prism enhanced position detection scheme provides a simple solution when the particle's independent movement direction and measurement direction are not parallel, which may happen in a special beam trap^[24].

This work was supported by the Science Challenge Project (No. TZ2018003), the National Natural Science Foundation of China (Nos. 61522508 and 91536219), and the Anhui Initiative in Quantum Information Technologies (No. AHY130000).

References

1. L. Neukirch and N. Vamivakas, *Contemp. Phys.* **56**, 48 (2015).
2. T. Li, S. Kheifets, D. Medellin, and M. G. Raizen, *Science* **328**, 1673 (2010).
3. E. Hebestreit, M. Frimmer, R. Reimann, and L. Novotny, *Phys. Rev. Lett.* **121**, 063602 (2018).
4. G. Ranjit, M. Cunningham, K. Casey, and A. Geraci, *Phys. Rev. A* **93**, 053801 (2016).
5. D. Hempston, J. Vovrosh, M. Toroš, G. Winstone, M. Rashid, and H. Ulbricht, *Appl. Phys. Lett.* **111**, 133111 (2017).
6. T. Li, S. Kheifets, and M. Raizen, *Nat. Phys.* **7**, 527 (2011).
7. J. Gieseler, B. Deutsch, R. Quidant, and L. Novotny, *Phys. Rev. Lett.* **109**, 103603 (2012).
8. L. Rondin, J. Gieseler, F. Ricci, R. Quidant, C. Dellago, and L. Novotny, *Nat. Nanotechnol.* **12**, 1130 (2017).
9. J. Gieseler and J. Millen, *Entropy* **20**, 326 (2018).
10. L. Neukirch, E. von Haartman, J. Rosenholm, and N. Vamivakas, *Nat. Photonics* **9**, 653 (2015).
11. T. Delord, P. Huillery, L. Schwab, L. Nicolas, L. Lecordier, and G. Hétet, *Phys. Rev. Lett.* **121**, 053602 (2018).
12. S. Bose, A. Mazumdar, G. Morley, H. Ulbricht, M. Toroš, M. Paternostro, A. Geraci, P. Barker, M. S. Kim, and G. Milburn, *Phys. Rev. Lett.* **119**, 240401 (2017).
13. M. Scala, M. S. Kim, G. W. Morley, P. F. Barker, and S. Bose, *Phys. Rev. Lett.* **111**, 180403 (2013).
14. Z. Yin, N. Zhao, and T. Li, *Sci. China Phys. Mech. Astron.* **58**, 1 (2015).
15. I. Chavez, R. Huang, K. Henderson, E.-L. Florin, and M. Raizen, *Rev. Sci. Instrum.* **79**, 105104 (2008).
16. M. Allersma, F. Gittes, M. DeCastro, R. Stewart, and C. Schmidt, *Biophys. J.* **74**, 1074 (1998).
17. F. Gittes and C. Schmidt, *Opt. Lett.* **23**, 7 (1998).
18. A. Pralle, M. Prummer, E. L. Florin, E. H. Stelzer, and J. K. Hörber, *Microsc. Res. Tech.* **44**, 378 (1999).
19. A. Rohrbach and E. Stelzer, *J. Appl. Phys.* **91**, 5474 (2002).
20. L. Novotny and B. Hecht, *Principles of Nano-Optics* (Cambridge University Press, 2006).
21. E. Hecht and A. Zajac, *Optics* (Addison-Wesley, 1974).
22. K. Berg-Sørensen and H. Flyvbjerg, *Rev. Sci. Instrum.* **75**, 594 (2004).
23. S. A. Beresnev, V. G. Chernyak, and G. A. Fomyagin, *J. Fluid Mech.* **219**, 405 (1990).
24. Z. Liu, T. Wang, Y. Zhang, X. Tang, P. Liu, Y. Zhang, X. Yang, J. Zhang, J. Yang, and L. Yuan, *Chin. Opt. Lett.* **16**, 053501 (2018).